Co-Sponsored by: FDA U.S. FOOD & DRUG ADMINISTRATION

Poster Abstracts and Poster Schedule

Noon–1:30 pm

Networking Lunch and Posters in the Exhibit Hall

1:00 pm-1:30 pm Authors (Posters 111-120) available for Questions and Answers

Poster 111 ***High Throughput LC-MS/MS Method for Determination of Efavirenz in Human Plasma***

Poster 112 ***Investigation of Inhibitor Preincubation Condition on Human OATP1B1, P -gp and BCRP Transporter In Vitro Inhibitory Potencies***

Poster 113 ***Time-Dependent Inhibition Demonstrated across Multiple Classes of Uptake Transporters***

Poster 114 ***Effects of Single-Nucleotide Variants in the Intracellular Loop 1 (ICL1) of ABCG2***

Poster 115 ***Molecular Interactions and Size Restrictions in the Binding and Transport of Drugs by Human Solute Carriers***

Poster 116 ***C-DILI™ Assay: Integrating BSEP Inhibition and FXR Antagonism to Improve Prediction of Cholestatic Drug Induced Liver Injury***

Poster 117 ***In Vitro Assessment of Transporter Interactions of PI3K/mTOR Inhibitor, LY3023414, for Potential for Clinical Implications***

Poster 118 ***Effect of a Common Genetic Variant (p.V444A) in the Bile Salt Export Pump on the Kinetics and Inhibition of Bile Acid Transport***

Poster 119 ***Functional Screening of Renal Drug Transporters Activity in Cryopreserved Human Proximal Tubule Epithelial Cells***

Poster 120 ***Sex Differences in Functional Expression of Organic Anion Transporting Polypeptide 1a4 (Oatp1a4) at the Blood-Brain Barrier in Sprague-Dawley Rats***

5:30 pm–7:00 pm

Reception and Posters in the Exhibit Hall

6:30 pm–7:00 pm Authors (Posters 111-120) available for Questions and Answers

Poster Abstracts and Poster Schedule

Tuesday, April 17, 2018

Poster Podium Schedule

8:00 am–8:10 am
Introduction to Poster Presentations
Arthur "Audie" Roberts, Ph.D., University of Georgia

8:10 am–8:30 am
Poster 105 ***Epigenetic Regulation of the MDR1 Transporter at the Human Blood-Brain Barrier: Interplay Between Histone Acetylation and Aryl Hydrocarbon Receptor Signaling***
Dahea You, Rutgers University

8:30 am–8:50 am
Poster 104 ***Assessing OATP1B1- and OATP1B3-Mediated Drug-Drug Interaction Potential of Vemurafenib Using Static and Physiologically Based Pharmacokinetic Models***
Taleah Farasyn, University of Oklahoma Health Sciences Center

8:50 am–9:10 am
Poster 102 ***Interactions of Bile Acids and Liver Injury-Associated Drugs with Organic Solute Transporter***
James John Beaudoin, University of North Carolina, Chapel Hill

9:10 am–9:30 am
Poster 106 ***Altered Hepatic and Renal Drug Transporter Expression and Endogenous Coproporphyrin I and III Concentrations in Serum and Urine of Polycystic Kidney Rats***
Jacqueline Bezencon, UNC Eshelman School of Pharmacy

9:30 am–9:50 am
Poster 103 ***Spatial and Sex Differences in the Intestinal Expression of Monocarboxylate Transporters***
J. Cao, University of the Pacific

9:50 am–10:10 am
Poster 101 ***Elucidation of Substrate-Binding Interactions Within Human Organic Cation Transporter 2 (SLC22A2) Through Homology Modeling***
Raymond E. Lai, Virginia Commonwealth University

Noon–1:30 pm

Networking Lunch and Posters in the Exhibit Hall

1:00 pm–1:30 pm Authors (Posters 101-110) available for Questions and Answers

Poster 101 *Elucidation of Substrate-Binding Interactions Within Human Organic Cation Transporter 2 (SLC22A2) Through Homology Modeling*

Poster 102 *Interactions of Bile Acids and Liver Injury-Associated Drugs with Organic Solute Transporter α/β*

Poster 103 *Spatial and Sex Differences in the Intestinal Expression of Monocarboxylate Transporters*

Poster 104 *Assessing OATP1B1- and OATP1B3-Mediated Drug-Drug Interaction Potential of Vemurafenib Using Static and Physiologically Based Pharmacokinetic Models*

Poster 105 *Epigenetic Regulation of the MDR1 Transporter at the Human Blood-Brain Barrier: Interplay between Histone Acetylation and Aryl Hydrocarbon Receptor Signaling*

Continued from Page 2

Poster 106 *Altered Hepatic and Renal Drug Transporter Expression and Endogenous Coproporphyrin I and III Concentrations in Serum and Urine of Polycystic Kidney Rats*

Poster 107 *Physiologically-Based Pharmacokinetic Modeling of the Effect of Chronic Kidney Disease on the Pharmacokinetics of Drugs Eliminated Nonrenally by CYP2C8 and OATP1B*

Poster 108 *Functional Expression of MRP1 in Human Distal Lung Epithelium and Its Interaction with Inhaled Drugs In Vitro*

Poster 109 *The Influence of Dissolution, PMAT Influx, and MATE Efflux Rates on Paracellular Absorption of Metformin Using a Mechanistic Oral Absorption/PBPK Model*

Poster 110 *Transgene Expression and Antigen Presentation from Non-viral Vectors Fabricated with DNA-Natural and DNA-Synthetic Condenser Lipid-Nano Particles in Dendritic Cell*

5:30 pm–7:00 pm

Reception and Posters in the Exhibit Hall

6:00 pm–7030 pm Authors (Posters 101-110) available for Questions and Answers

In Vitro Assessment of Transporter Interactions of PI3K/mTOR Inhibitor, LY3023414, for Potential for Clinical Implications

Ryan Brackman, Shelby Hullett, Lisa Hong Chen, Lian Zhou, David W. Bedwell, Kathleen M. Hillgren, Y. Anne Pak
Eli Lilly and Company

Purpose: The class I phosphatidylinositol-3-kinase-protein kinase B-mammalian target of rapamycin (P13K/mTOR) pathway regulates the cell cycle and is altered in cancer cell growth and survival. LY3023414 is an orally available, potent, small molecule dual kinase inhibitor of PI3K/mTOR, and is being investigated as a potential treatment for patients with non-small cell lung cancer or prostate cancer in clinical trials. LY3023414 is primarily cleared by liver. Therefore, substrate potential of LY3023414 for hepatic solute carrier (SLC) transporters, OATP1B1, OATP1B3, and OCT1 was investigated. Additionally, the ability of LY3023414 to inhibit a set of clinically relevant hepatic and renal SLC transporters was assessed using a panel of in vitro cell lines.

Methods: Stably transfected human embryonic kidney (HEK) cells expressing human Organic Cation Transporter 1 (OCT1), OCT2, Organic Anion Transporter 1 (OAT1), OAT3, Multidrug and Toxin Extrusion protein 1 (MATE1), MATE2-K, and virally transduced HEK cell lines overexpressing human Organic Anion Transporting Polypeptide 1B1 (vOATP1B1), and vOATP1B3 were used to determine if LY3023414 is a substrate and/or inhibitor of these transporters. MATE1 and MATE2-K cells were purchased from Corning. Additionally, selected inhibitors of OCT1-mediated LY3023414 uptake were compared with inhibition of prototypical OCT1 substrates, metformin and sumatriptan, to evaluate 1) inhibition potency of these inhibitors, and 2) if inhibitions are substrate-dependent.

Results: Clinically relevant LY3023414 inhibitions were observed for efflux transporters, MATE1 and MATE2K, hepatic uptake transporters, OATP1B1, OATP1B3, and OCT1, and renal uptake transporters, OAT3 and OCT2. No clinically relevant inhibition was observed with renal uptake transporter OAT1. LY3023414 is a substrate of hepatic uptake transporter, OCT1, but not a substrate of hepatic uptake transporters, OATP1B1 and OATP1B3. Several clinically relevant OCT1 inhibitors were tested to investigate the inhibition potential of OCT1-mediated uptake of LY3023414 and varying degrees of inhibition were observed. Ondansetron and Palonosetron had different OCT1 IC_{50} values when using LY3023414 as a substrate compared to metformin or sumatriptan. Conversely, verapamil showed similar OCT1 IC_{50} values when metformin, sumatriptan, and LY3023414 were used as substrates.

Conclusion: Clinically relevant drug inhibitions may occur when LY3023414 is co-administered with substrates of MATE1, MATE2K, OATP1B1, OATP1B3, OCT1, OAT3, and OCT2. LY3023414 is a substrate of OCT1, but not a substrate OATP1B1 and OATP1B3. Verapamil may have a clinically relevant effect on the disposition of LY3023414. Finally, substrate specificity should be considered when evaluating interaction potential as some inhibitor/substrate combinations appear to show specificity in the OCT1 transporter.

Sex Differences in Functional Expression of Organic Anion Transporting Polypeptide 1a4 (Oatp1a4) at the Blood-Brain Barrier in Sprague-Dawley Rats

Patrick T. Ronaldson, Wazir Abdullahi, Bianca G. Reilly, Hrvoje Brzica
University of Arizona

Purpose: The blood-brain barrier (BBB) is a physical and biochemical barrier between the blood and the brain that restricts central nervous system (CNS) delivery of endogenous and exogenous compounds. In terms of pharmacotherapy, the BBB limits treatment options for multiple life-threatening diseases such as ischemic stroke, a leading cause of mortality and long term morbidity. Therefore, there is a critical need to identify and characterize novel paradigms for CNS drug delivery in ischemic stroke. One such approach is to target endogenous BBB transporters such as organic anion transporting polypeptide 1a4 (Oatp1a4), which is known to transport therapeutics with neuroprotective properties such as -hydroxyl-3-methylglutaryl coenzyme A (HMG CoA) reductase inhibitors (i.e., statins). In order to advance targeting of Oatp1a4 as a therapeutic strategy for ischemic stroke, it is critical to characterize differences in expression and/or function of this transporter at the BBB based on sex. Indeed, evidence in the scientific literature indicates that differences in Oatp1a4 mRNA and protein in liver exist between males and females; however, similar studies have not been conducted in the brain. The goal of the present study was to investigate, *in vivo*, sex differences in functional expression of Oatp1a4 at the BBB and to determine the role of sex hormones in Oatp1a4 regulation.

Methods: Sex differences in Oatp1a4 expression and activity were studied in adult Sprague-Dawley rats as well as in prepurbertal (i.e., 6-week-old) Sprague-Dawley rats. To determine the role of sex hormones on Oatp1a4 expression, 6-week-old rats were subjected to gonadectomy and housed for an additional 10 weeks to enable these animals to develop in the absence of sex hormones. Immunofluorescence microscopy on paraformaldehyde (4%)-fixed brain tissue was used to study Oatp1a4 cellular localization. Western blot analyses on isolated brain microvessels was used to examine protein expression of Oatp1a4 at the BBB. *In situ* brain perfusion studies using [^{3}H]taurocholate (1.0 µCi/ ml perfusate), an established Oatp1a4 substrate, was used to determine if changes in Oatp1a4 protein expression correlated with changes in transport activity.

Results: Immunofluorescence microscopy confirmed Oatp1a4 localization in brain microvessels in both male and female animals. In both sexes, western blot analyses revealed the presence of a single band at a molecular weight previously reported for Oatp1a4. Oatp1a4 protein expression in brain microvessels was significantly higher (5-fold) in females as compared to males. Similarly, quantitative real-time PCR analysis showed increased (greater than 3-fold) mRNA expression for *Slco1a4* (i.e., the gene that encodes Oatp1a4) in brain microvessels isolated from female rats. Oatp1a4 protein expression was enhanced in castrated male animals but was not affected by ovariectomy in female animals. In prepubertal rats, there was no difference in Oatp1a4 protein expression between male animals and female animals. Brain accumulation of [^{3}H]taurocholate in male rats was increased following castration as compared to sham-operated controls. In contrast, there was no difference in brain uptake of [^{3}H]taurocholate between ovariectomized female rats and sham-operated controls.

Conclusions: These data show, for the first time, biological variability in Oatp1a4 functional expression at the BBB based on sex. Such findings may have profound implications for CNS drug delivery in the treatment of diseases such as ischemic stroke. Studies are ongoing to fully characterize sex differences in the molecular pathways involved in regulation of Oatp1a4 expression and activity.

High Throughput LC-MS/MS Method for Determination of Efavirenz in Human Plasma

Murali Javvaji
Teva Pharmaceuticals, USA

Purpose: To develop and validate an LC/MS/MS method for the determination of EFAVIRENZ in Human plasma.

Method: Efavirenz (EFV) is a non-nucleoside reverse transcriptase inhibitor (NNRTI) which is used in the treatment of human immunodeficiency virus type 1 (HIV-1). It is generally used in combination with other drugs as a part of highly active antiretroviral therapy (HAART). The aim of the current study was to develop a selective and sensitive LCMS/MS method with relatively low run time for its application to a bioequivalence study. As part of it developed an isocratic LC-MS/MS method with a LOQ of 5 ng/mL using atazanavir (ATZ) as internal standard. The method uses a highly selective solid phase extraction technique for sample preparation. Positive electrospray ionization with a mobile phase containing methanol : 0.1% formic acid in water (90:10, v/v) was used to detect the drugs. During method development more emphasis was given to establish a simple and fast processing method with minimal matrix effects. No cross interference was observed between the analyte and ISTD. The method utilizes a processing volume of 0.2 mL and injection volume of 10 µL. The chromatographic run time was 3.2 min.

Results: Selection of internal standards Selection of internal standard is highly important in the development of reliable and precise analytical method. ATZ was selected based on its close partition coefficient (~4.5) value with the analyte. ATZ has shown consistent recoveries along with analyte and more importantly, its chromatographic behavior was almost similar with analyte (with same RT of 2.2 min.) and resulted in minimal matrix suppressions. Optimization of mass spectrometric conditions Method development was initiated with scanning of the compounds for parent and product ions to perform multiple reaction monitoring. 250 ng/mL solutions of EFV and ATZ were separately prepared in 50% methanol and are infused using a syringe pump at a rate of 10 µL/min. Based on their ability to accept the protons, analyte and ISTD was tuned in positive mode using electrospray ionization technique. The mass spectral scanning was performed over the range of 100 to 800 amu. After selecting the parent and stable product ion, compound and gas parameters were optimized in flow injection analysis. In the mass spectrometer, zero air was used as source gas and pure nitrogen was used as collision gas. ESI negative ionization mode was not verified as the analyte does not have proton donar functional groups. The [M+H]+ peaks were observed at m/z of 316.4 for EFV and at 705.6 for ATZ. The abundant product ions were found at m/z of 244.3 for EFV and at 335.3 for ATZ (Figure 4.1), by applying appropriate collision energy. In EFV additional product ions at m/z of 272, 237, 232 and 168 were also observed, however they were not selected as the response with m/z of 244.3 is sufficient to achieve the desirable LOQ. During the optimization of compound parameters comparatively high collision energy was applied for ATZ due to its complex structure. Change of source temperature between 350 to 500 °C does not shown significant impact signal intensities. Ionspray voltage at 5200 V was found appropriate and a 10% change in its value resulted in drastic decrease in the signal intensities. LC conditions for analyte and ISTD were set under isocratic mode. Optimization of mobile phase was initiated with methanol and milli-Q water. Replacement of milli-Q water with 0.1% formic acid in water has augmented the analyte response by 200%, however no significant increase was identified in ATZ response. Incorporation of buffer even at 1 mM concentration has shown a negative impact on signal intensities. Use of methanol in mobile phase has provided comparatively high and consistent response ratios for analyte and ISTD. During the optimization of stationary phase Zodiac C18 (100 X 3.0, 3 µm) and Oyster ODS3 (100 X 4.6, 5 µm) columns were verified. Oyster ODS3 has given a more selective chromatography with symmetrical peaks. C8 columns has produced as highly tailed chromatographic peaks with retention time at 2.0 min. A flow rate of 0.8 mL/min was used to minimize the run time and a post column splitness of 30:70 was used without compromise in the peak responses.

Conclusion: A simple, rapid and rugged LC–MS/MS method was developed and validated for the determination EFV in human K2 EDTA plasma. The method validation [12-15] was performed as per USFDA and EMA guidelines and has comfortably met the acceptance criteria. The MRM transitions were made with positive electrospray ionization at m/z 316.6 → 244.3 for EFV and at m/z 705.6 → 335.3 for ATZ (ISTD), with a dwell time of 200 ms per transition.

Transgene Expression and Antigen Presentation from Non-viral Vectors Fabricated with DNA-Natural and DNA-Synthetic Condenser Lipid-nano Particles in Dendritic Cell

Sharif M. Shaheen[1, 2], Md. Jashim Uddin[3], M. Mustafezur Rahman[2], A. K. Azad[2]
[1]Hokkaido University; [2]Daffodil International University; [3]Vanderbilt University

Purpose: Gene therapy depends on the DNA delivery perfectly to the nuclear subdomain, and DNA should be orchestrated in a lipid based programmed packaging like multi-functional envelope type of nano device (MEND) and tetra lamellar multi-functional envelope type of nano device (T-MEND) published elsewhere. In both the packaging system, DNA has to make a complex (core) with a cationic polymer. It is important how about the effect of such a DNA/condenser core inside the programmed-packaging reflects the transgene expression.

Methods: Here we compared transgene expression of a firefly luciferase gene from both the protaplex (protamine-DNA) and rotaplex (polyrotaxane-DNA), packaged in MENDs. Dendritic cells were transfected with these nanoparticles and transgene expression, cell viability as well as antigen presentations were measured.

Results: Transgene expression from the MEND of protaplex was significantly higher in JAWs-II cell (dendritic cell line) and bone marrow dendritic cell. Cell viability and antigen presentations from the protaplex were also prompt and better than that of polyplex, when T-MEND package systems containing protaplex and rotaplex, were compared. Confocal microscopic studies of fluorescently labeled plasmid DNA reflected the evidence of ease decondensation of DNA from the protaplex than that of a rotaplex.

Conclusion: Our results suggest that a natural DNA condenser (protamine in protaplex) prefers transgene expression as well as antigen presentation better to those of synthetic polycationic condenser (polyrotaxane in rotaplex).

C-DILI™ Assay: Integrating BSEP Inhibition and FXR Antagonism to Improve Prediction of Cholestatic Drug Induced Liver Injury

Jonathan P. Jackson, Matthew K. Palmer, Caroline L. Moseley, Christopher B. Black, and Kenneth R. Brouwer
BioIVT, ADME-TOX Division

Purpose: Cholestatic DILI in humans has been associated with bile salt export pump (BSEP) inhibition; however, *in vitro* BSEP IC_{50} concentrations do not correlate with *in vivo* cholestatic DILI severity. Sandwich-cultured human hepatocytes (SCHH) when treated with BSEP inhibitors respond to the resulting increased intracellular concentration (ICC) of bile acids (BA), by activation of FXR (adaptive response). This results in decreased synthesis of BA and increased expression of basolateral and canalicular efflux transporters for BA via OST alpha/beta, and BSEP which prevents cholestatic hepatotoxicity. We determined the time course of this adaptive response, changes in the ICC of BA, the effects of FXR antagonists, the *in vivo* relevance, and whether integration of FXR regulatory effects would improve the prediction of cholestatic DILI.

Methods: Cryopreserved, Transporter Certified™ human hepatocytes in a sandwich configuration were cultured using QualGro ™ Media for 5 days. On Day 5 of culture, the time course of the adaptive response was determined by determining the effect of cyclosporine A on the biliary excretion, and ICC of bile acids (LCMS analysis), in parallel with FXR activation (gene expression - TaqMan® primer/probe sets). Mechanistic modeling was used to determine the functional effects of mRNA-based changes in FXR activation on the hepatobiliary disposition of bile acids. The effect of FXR antagonists (troglitazone, DY268) on the FXR mediated activation of basolateral efflux transport were also evaluated. 50 compounds with varying degrees of BSEP inhibition and DILI (NIH LiverTox database) were evaluated (24 hr exposure) for their potential to impact this adaptive response.

Results: Cyclosporine A decreased the biliary excretion of endogenous bile acids in a time dependent manner, with a parallel increase in the ICC of BA, followed by activation of FXR. FXR activation resulted in a 2X increase in the biliary efflux clearance, and a 6X increase in the basolateral efflux clearance (adaptive response). Co-administration of FXR antagonists reduced the FXR mediated response by 50 and 95% for troglitazone and DY268, respectively. Integration of the effect on the adaptive response in addition to the effect on BSEP inhibition improved the accuracy for prediction of cholestatic DILI from 22% (BSEP inhibition alone) to 93%.

Conclusion: In addition to BSEP inhibition, integration of inhibition of basolateral efflux and/or interference with the adaptive response (FXR antagonism) allows for more accurate prediction of cholestatic DILI.

Functional Expression of MRP1 in Human Distal Lung Epithelium and its Interaction With Inhaled Drugs *In Vitro*

M. A. Selo[1,2], L. Springer[2], S. Nickel[2], C. Ehrhardt[2]
1. University of Kufa, Faculty of Pharmacy, 2. Trinity College Dublin, School of Pharmacy and Pharmaceutical Sciences

Purpose: Multidrug resistance-associated protein 1 (MRP1) has been identified to have high protein abundance in human lung tissues. The subcellular localisation and functional activity of the transporter in distal lung epithelium, however, remains poorly investigated. The aim of this project was to investigate the expression, subcellular localisation and activity of MRP1 in freshly isolated human alveolar epithelial type 2 (AT2) and type 1-like (AT1-like) cells in primary culture and in the NCI-H441 cell line and to assess the effect of inhaled drugs on MRP1 expression and activity *in vitro.*

Method: MRP1 expression in AT2 and AT1-like cells from three different patients as well as over the course of 30 passages of NCI-H441 cells was studied using q-PCR and immunoblot. Confocal laser scanning microscopy and cell surface biotinylation were used to confirm transporter localisation. Transporter activity was assessed by bidirectional transport and efflux studies of the MRP1 substrate, 5(6)-carboxyfluorescein (CF) (converted intracellularly from 5(6)-carboxyfluorescein-diacetate, CFDA) across/from monolayers of AT1-like and NCI-H441 cells. Furthermore, the effect of budesonide and salbutamol on MRP1 expression and CF(DA) efflux were investigated.

Results: MRP1 protein abundance increased upon differentiation of AT2 to AT1-like phenotype, however, ABCC1 gene expression remained constant. MRP1 was found to be stably expressed in NCI-H441 cells, regardless of passage number and cell culture conditions, at similar levels to those observed in AT1-like cells. The transporter was confirmed to be localised to the basolateral membrane of both cell models. Bidirectional transport studies across monolayers of ATI-like and NCI-H441 cells showed MK-571 sensitive net absorption of CF. Budesonide decreased CF efflux at a concentration-dependent manner without influencing MRP1 abundance, whereas salbutamol had no effect.

Conclusion: MRP1 abundance increases upon transdifferentiation of human AT2 to AT1-like cells in primary culture. In AT1-like and NCI-H441 cells, transporter expression levels, localisation and activity are comparable, thus, the cell line is a useful *in vitro* model to study MRP1 in distal lung epithelium. Furthermore, budesonide reduces MRP1 activity *in vitro*.

Investigation of inhibitor preincubation condition on human OATP1B1, P-gp and BCRP transporter *in vitro* inhibitory potencies

Hayley Atkinson, Valentin Clements, Jennifer Meadows, Sam Outteridge, Sarah Pickering, Amy Radcliffe and Robert Elsby
Cyprotex

Purpose: To evaluate whether the determined *in vitro* IC_{50} versus OATP1B1 following a 15 min preincubation step with inhibitor is comparable to that determined following a 30 min preincubation step with inhibitor [1], and determine whether inhibitor preincubation impacts on *in vitro* IC_{50} values determined in polarised cell monolayers versus P-gp and BCRP.

Methods: Investigations comparing inhibitor preincubation times were conducted in HEK293 cells overexpressing OATP1B1 and corresponding vector control cells. Following a 15 min or 30 min preincubation step with inhibitor, uptake of probe substrate [^{3}H]estradiol glucuronide (0.02 µM) was determined over 2 min in the absence and presence of either cyclosporin A (0.01-10 µM) or atorvastatin (0.01-30 µM). To investigate the impact of inhibitor preincubation on *in vitro* IC_{50} values determined for P-gp or BCRP, unidirectional (basolateral-to-apical) flux of probe substrate [^{3}H]digoxin (5 µM), or [^{3}H]estrone sulfate (1 µM), was assessed across polarised MDCK-MDR1, or Caco-2 cells, respectively. Incubations (90 min) were performed in the absence or presence of inhibitor, following a 30 min preincubation step with either inhibitor or buffer alone. Inhibitors included cyclosporin A (0.01-10 µM), elacridar (0.003-3 µM), ketoconazole (0.1-100 µM) or verapamil (0.1-100 µM) for P-gp and novobiocin (0.1-100 µM) and fumitremorgin C (0.01-10 µM) for BCRP. Each set of incubation conditions utilised the same inhibitor solutions and were performed using triplicate wells per inhibitor concentration over multiple occasions.

Results: Cyclosporin A caused equipotent inhibition of OATP1B1-mediated transport following either a 15 min preincubation step with inhibitor (mean IC_{50} = 0.330 µM) or a 30 min preincubation step with inhibitor (mean IC_{50} = 0.340 µM). A similar result was observed for atorvastatin which inhibited OATP1B1 with a mean IC_{50} value of 0.260 µM or 0.269 µM, following a 15 min or 30 min preincubation with inhibitor, respectively. For BCRP, preincubation of Caco-2 cells with inhibitor, compared to preincubation with buffer alone, had no impact on the determined IC_{50} values for novobiocin or fumitremorgin C. Conversely for P-gp, whilst preincubation of MDCK-MDR1 cells with inhibitor resulted in only a small shift (decrease) in the determined mean IC_{50} values for cyclosporin A (1.63 µM to 0.968 µM) and ketoconazole (14.9 µM to 8.83 µM) compared to preincubation with buffer alone, these changes were not statistically significant. Furthermore, no difference in IC_{50} was observed for verapamil. Only elacridar exhibited a significant 2.9-fold decrease in mean IC_{50} (0.814 µM to 0.284 µM) following inhibitor preincubation.

Conclusions: Based on the OATP1B1 probe substrate and reference inhibitor combinations utilised in this study, our observations indicate that a 15 min preincubation step with inhibitor produces the same degree of inhibition (IC_{50}) against OATP1B1 as the 30 min preincubation period suggested in the current FDA draft guidance (2017). Furthermore, whilst an inhibitor preincubation step may possibly be deemed necessary for certain compounds when assessing inhibition of P-gp-mediated transport in MDCK-MDR1 cell monolayers, it does not appear to be a necessary requirement when studying inhibition of BCRP in Caco-2 cell monolayers.

[1] Elsby R, Chidlaw S, Outteridge S, Sullivan R and Pickering S. (2016) Further investigation of the impact of inhibitor pre-incubation on human OATP1B1, OAT3, OCT2 and MATE1 transporter *in vitro* inhibitory potencies. The AAPS Journal (M1022), available from http://www.aapsj.org.

Elucidation of Substrate-Binding Interactions Within Human Organic Cation Transporter 2 (SLC22A2) Through Homology Modeling

R. E. Lai, P. D. Mosier, D. H. Sweet
Virginia Commonwealth University

Purpose: To elucidate the critical amino acid residues for transporter-substrate binding interactions on human (h)OCT2 through *in silico* molecular modeling techniques (homology modeling and automated docking), as well as *in vitro* mutagenesis and kinetic transport experiments.

Methods: Homology models of the tertiary structure of hOCT2 were generated using the known high-resolution crystal structure of *Piriformospora indica* phosphate transporter (PiPT) serving as the template. Amino acid sequence alignment of hOCT2 with the template and subsequent generation of a population of 100 homology models were performed using ClustalX 2.1 and MODELLER v9.14, respectively. The prototypical hOCT2 substrate, 1-methyl-1-phenylpyridinium (MPP^+), was sketched and energy-minimized using SYBL-X 2.1 (Tripos Force Field, Gasteiger-Hückle charges distance-dependent dielectric constant = 4.0 D/Å) and docked into each of the 100 models using GOLD Suite 5.4. A favorable interaction model was selected based on the combined MODELLER DOPE score, GOLD docking score, and Ramachandran plot outliers. High resolution images were obtained using PyMOL v1.8. For *in vitro* studies, single amino acid substitutions were introduced into hOCT2 using the PCR-based QuikChange Lightning mutagenesis kit and synthetic oligonucleotide primers. All hOCT2 constructs were verified via DNA sequencing. Stable transfection of the mutants with 1µg plasmid DNA using cationic lipid-based transfection was performed in Chinese Hamster Ovary (CHO) cells. The Michaelis-Menten constant (K_m) was determined for MPP^+ in each of the generated mutant hOCT2-expressing cell lines via saturation analysis where 2 $x10^5$ cells per well were grown in anti-biotic free conditions for 48 hours in a 24-well plate then treated with transport buffer containing 1-200 µM [^{3}H] MPP^+ (0.25 µCi/mL) for 1 min. All data were corrected for non-hOCT2-mediated background accumulation in empty vector control cells and reported as mean ± SD. Statistical differences were assessed using the unpaired two-tailed Student's t-test. A difference was deemed statistically significant if $p<0.05$.

Results: The selected *in silico* MPP^+-hOCT2 interaction model identified five amino acids (Gln242, Tyr245, Thr246, Tyr362, and Glu448) as potential candidates critical for transporter-MPP^+ binding interactions. Within the proposed binding pocket, hydrophobic interactions were identified between MPP^+ and amino acid residues Gln242, Thr246, and Glu448, and one of the aromatic rings of MPP^+ was found to be involved in edge-face pi and pi-stacking interactions with Tyr245 and Tyr362, respectively. In addition, we previously reported that transport activity was completely abolished by an Asp478 mutation in hOCT3 (Liu *et al.* AAPS 2016). From the functional screening study, the hOCT2 Asp475Glu mutant showed no difference from wild-type hOCT2 in transport activity of the MPP^+ substrate (p-value >0.05). However, in stark contrast to our previous hOCT3 results, substrate affinity for the hOCT2 Asp475Glu mutant was not significantly different from wild-type hOCT2 (K_m= 13.5 ± 7 µM and 16 ± 3 µM, respectively, p-value > 0.05). Correspondingly, the hOCT2 homology model revealed that amino acid Asp475 was outside the proposed binding pocket.

Conclusions: The prototypical substrate MPP^+ was docked into a population of hOCT2 homology models. Using the most favorable model, several amino acid residues potentially involved in MPP^+-hOCT2 binding interactions were identified. However, despite a high degree of sequence similarity (70%) and identity (51%) between hOCT2 and hOCT3, the conserved aspartic acid residue (position 475 in hOCT2 and position 478 in hOCT3) previously demonstrated to be essential for MPP^+ interactions with hOCT3 appears to exert no influence on MPP^+ interactions with hOCT2. This finding was supported by our hOCT2 *in silico* model wherein Asp475 was located outside of the binding pocket. The difference in transporter function and affinity observed between hOCT3 Asp478Glu and hOCT2 Asp475Glu suggests that the critical residues for MPP^+-transporter interaction may vary depending on the OCT paralog, even for the same substrate. Future work will involve introducing a series of conservative and non-conservative point mutations into hOCT2 based on the amino acid residues identified in this study; these will subsequently be evaluated with *in vitro* kinetic studies. Additionally, molecular modeling studies will be performed using other substrates with different chemical structures to investigate and identify alternatively and/or additionally relevant residues in hOCT2.

Physiologically-Based Pharmacokinetic Modeling of the Effect of Chronic Kidney Disease on the Pharmacokinetics of Drugs Eliminated Nonrenally by CYP2C8 and OATP1B

Ming-Liang Tan[1], Ping Zhao[1,2], Lei Zhang[1], Yunn-Fang Ho[3], Manthena V. S. Varma[4], Sibylle Neuhoff[5], Thomas D. Nolin[6], Aleksandra Galetin[7] and Shiew-Mei Huang[1]
[1]U.S. Food and Drug Administration; [2]Bill and Melinda Gates Foundation; [3]National Taiwan University; [4]Pfizer Inc.; [5]Simcyp (a Certara Company); [6]University of Pittsburgh; [7]University of Manchester

Purpose: To employ physiologically-based pharmacokinetic (PBPK) modeling to understand the possible effect of chronic kidney disease (CKD) on CYP2C8 and/or OATP1B that may explain changes in exposure of 4 drugs metabolized by CYP2C8 and/or transported by OATP1B in CKD patients: rosiglitazone, pioglitazone, pitavastatin and repaglinide.

Methods: The base PBPK models for these 4 drugs were adopted using a PBPK platform (Simcyp, V16). The models were verified and optimized using clinical drug-drug interaction and pharmacogenetics data from the literature. Then, plasma PK profiles of these 4 drugs were simulated in severe CKD patients considering well-documented pathophysiological indices in this population, such as changes in glomerular filtration rate and plasma protein binding, together with modification of activity of either CYP2C8 and/or OATP1B in a stepwise manner. The predictions were compared to the clinical data in CKD patients.

Results: See Table 1.

Conclusion: The PBPK analysis suggests that OATP1B activity is decreased in patients with severe CKD, while changes to CYP2C8 are negligible. This improved understanding of clearance pathway dependency change in CKD patients is important to inform the need to conduct clinical PK studies for optimal use of nonrenally eliminated drugs in CKD patients.

Table 1 Calculated and observed AUCR between severe CKD and health control (HC)

Drugs	fu*		Simulated total				Simulated unbound			
	HC	CKD	SimCYP default[a]	CKD 1[b] OATP 100%	CKD 1[c] OATP reduced	Observed total*	SimCYP default[a]	CKD 1[b] OATP 100%	CKD 1[c] OATP reduced	Observed unbound*
Rosiglitazone	0.0016	0.0022	1.44	0.86	NA	0.81	2.47	1.09	NA	1.11
Pioglitazone	0.03	*0.035***	1.58	0.89	NA	0.78	2.40	1.09	NA	*0.92***
Pitavastatin	0.006	0.006	0.85	1.00	1.36[d]	1.36	1.05	1.00	1.36[d]	1.36
Repaglinide	0.036	0.036	1.37	1.04	2.62[e]	2.72	1.72	1.08	2.72[e]	2.72

Severe CKD population used in the simulations: [a]SimCYP built-in "Sim-RenalGFR_less30" severe renal impairment patients with GFR < 30 mL/min, [b]SimCYP healthy controls (HC) with GFR, age, and sex matched to the corresponding clinical CKD studies, [c]SimCYP healthy HC with GFR, age, and sex matched to the corresponding clinical CKD studies and with reduced OATP1B1 abundance to match the clinical observation; [d]OATP1B1 abundance was reduced to 70% of the HC for pitavastatin (a OATP1B1 substrate) and [e]OATP1B1 abundance was reduced to 35% of the HC for repaglinide (a CYP2C8 and OATP1B1 dual substrate). *Observed fu and AUCR are from the same clinical studies as cited in Reference 2, unless otherwise noted. **fu estimated in Reference 2.

No reduction in CYP2C8 enzyme abundance or function was required to match the observed AUC change in severe CKD subjects for pioglitazone and rosiglitazone, while 30% reduction in OATP1B1 abundance or function was needed to match the AUC change in severe CKD subjects for pitavastatin. For CYP2C8 and OATP1B1 dual substrate repaglinide, 65% reduction in OATP1B1 abundance or function is needed to match the AUC change in severe CKD subjects.

References

1. K Yoshida, B Sun, L Zhang, P Zhao, DR Abernethy, TD Nolin, A Rostami-Hodjegan, I Zineh and S-M Huang, *Clin Pharmacol Ther* **100**, 75(2016).
2. M-L Tan, K Yoshida, P Zhao, L Zhang, TD Nolin, M Piquette-Miller, A Galetin and S-M Huang, *Clin Pharmacol Ther* http://onlinelibrary.wiley.com/doi/10.1002/cpt.1807/epdf

Time-Dependent Inhibition Demonstrated across Multiple Classes of Uptake Transporters

P. Tátrai[1], P. Schweigler[2], B. Poller[2], I. Hanna[2], Zs. Gáborik[1], and F. Huth[2]
[1]Solvo Biotechnology, Hungary; [2]Novartis, Switzerland

Purpose: To identify novel time-dependent (TD) inhibitors of uptake transporters *in vitro*.

Methods: HEK293 cells overexpressing uptake transporters OATP1B1/1B3, OAT1/3, OCT1/2, and MATE1/2-K were used to determine IC_{50} values of corresponding inhibitors with or without 3 hours of preincubation. A total of 64 transporter-inhibitor combinations were analyzed. A shift in IC50 greater than 2.5-fold (i.e., IC_{50} with preincubation ≤ 0.4 x IC_{50} without preincubation) was considered relevant. In addition, transwell permeability of the inhibitors across a low efflux MDCK cell (MDCK-LE) monolayer was measured.

Results: TD inhibition was observed, albeit with different frequencies, across all classes of uptake transporters investigated. The proportion of inhibitors tested positive with at least one member of a cognate transporter pair was 3/5 for OATP1B1/1B3, 1/10 for OAT1/3, 6/9 for OCT1/2, and 1/8 for MATE1/2-K. In particular, ledipasvir, an antiviral previously not recognized as an OCT inhibitor, was shown to potently suppress both OCT1 and 2 upon preincubation (IC_{50} with preincubation: 0.15 μM and 74.3 μM, respectively). MDCK-LE permeability of the inhibitors ranged between 0.012 and $16.9*10^{-6}$ cm/s, and compounds with low to medium P_{app} (≤ $5*10^{-6}$ cm/s) were more likely to show TD behavior, as such compounds were involved in 10/15, or 66.7%, of observed cases of TD inhibition. However, the association between MDCK-LE permeability and TD effect was not statistically significant. Among inhibitors that were non-substrates of their respective transporters, the magnitude of IC_{50} shift correlated positively with cLogP (Spearman's r = 0.43, P=0.008) and molecular weight (r = 0.67, P<0.0001).

Conclusion: Since TD behavior was seen not only in OATPs but also in OATs, OCTs, and MATEs, the phenomenon of TD transporter inhibition seems to extend beyond OATPs. Non-substrate inhibitors with high hydrophobicity and high molecular weight were more liable to exhibiting a TD effect, while TD inhibition was less typical of high MDCK-LE permeability compounds.

Table 1. Summary of IC_{50} shift experiments. HEK293 cells overexpressing uptake transporters were used to determine IC_{50} values without preincubation compared to a 3-hour preincubation in the presence of selected inhibitors. A total of 64 transporter-inhibitor pairs were analyzed. Time-dependent (TD) inhibition was defined as an IC_{50} shift ≥ 2.5 (IC_{50} with preincubation ≤ 0.4 x IC_{50} without preincubation). *Insufficient inhibition for IC_{50} calculation

	OATP1B1	OATP1B3	OAT1	OAT3	OCT1	OCT2	MATE1	MATE2-K
Failed inhibitors*	0	1	3	3	1	2	0	0
TD inhibitors, total	**2**	**2**	**0**	**1**	**6**	**6**	**0**	**1**
Substrates	1	1	0	0	0	1	0	0
Non-substrates	1	1	0	1	6	5	0	1
Non-TD inhibitors	**3**	**2**	**7**	**6**	**2**	**1**	**8**	**7**
Substrates	3	2	2	2	2	0	1	1
Non-substrates	0	0	5	4	0	1	7	6
Total inhibitors investigated	**5**	**5**	**10**	**10**	**9**	**9**	**8**	**8**

Figure 1. Time-dependent effect of ledipasvir on OCT1 and OCT2. IC_{50} values without preincubation could not be accurately calculated due to very weak (OCT1) or no (OCT2) inhibition of metformin transport. IC_{50} with preincubation was 0.15 μM and 74.3 μM, respectively, for OCT1 and OCT2. A conservatively estimated IC_{50} shift value of 10 was used in subsequent correlation analyses.

O C T 1

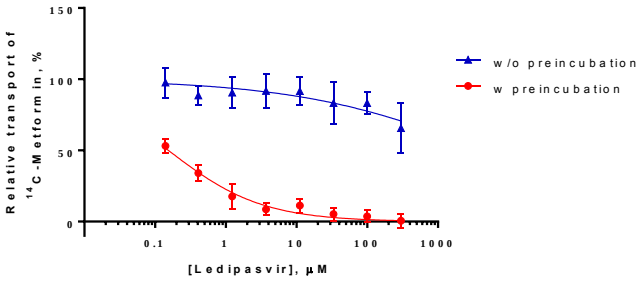

	w/o preincubation	w preincubation
IC50	4302	0.1543

O C T 2

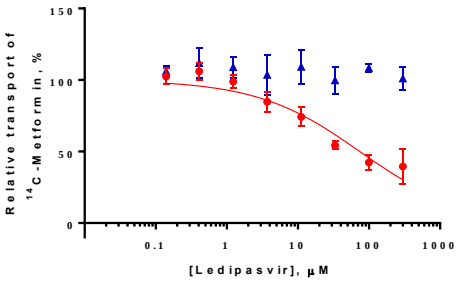

	w/o preincubation	w preincubation
IC50		74.26

Altered Hepatic and Renal Drug Transporter Expression and Endogenous Coproporphyrin I and III Concentrations in Serum and Urine of Polycystic Kidney Rats

Jacqueline Bezençon[1], Chitra Saran[2], James J. Beaudoin[1], Dong Fu[1], Sharin Roth[3], William Brock[4], Kim L. R. Brouwer[1]

[1] Division of Pharmacotherapy and Experimental Therapeutics, UNC Eshelman School of Pharmacy, University of North Carolina; [2] Office of Graduate Education, UNC School of Medicine, University of North Carolina; [3] Otsuka Pharmaceutical Development & Commercialization, Inc.; [4] Brock Scientific Consulting

Purpose: Autosomal dominant polycystic kidney disease (ADPKD) is an inheritable genetic disease and a leading cause of renal failure. In addition to renal cysts, patients with ADPKD often develop hepatic cysts, which may influence the disposition of endogenous [e.g., bile acids, coproporphyrin (CP)-I and CP-III] or exogenous compounds and could lead to altered efficacy or toxicity of medications. The polycystic kidney (PCK) rat is a model of polycystic kidney disease (PKD) and polycystic liver disease (PLD), and is used as a model for ADPKD. To gain insight into hepatic and renal transporter expression and function in PCK rats, mRNA and protein levels were measured, and CP-I and CP-III, transporter probes of organic anion transporting polypeptides (Oatps) and multidrug resistance-associated protein 2 (Mrp2), were analyzed in serum and urine of PCK and wild-type (WT) Sprague Dawley rats.

Methods: Membrane proteins from the livers and kidneys of PCK and WT rats (16-20 weeks old; *n*=3-4 per group) were extracted using a ProteoExtract® native membrane protein extraction kit. mRNA levels of Oatp1a1, Oatp2b1, Oatp1a4, Mrp3, Mrp2, organic solute transporter (Ost)α, Ostβ, and multidrug resistance protein 1 (Mdr1) were measured by qPCR in liver samples, and protein levels of Oatp1a1, Oatp2b1, Oatp1a4, Mrp3, Mrp2 in liver samples, and of Mrp2 and Mrp4 in kidney samples, were detected by western blot. In addition, a LC-MS/MS assay was developed and validated to quantify CP-I & CP-III concentrations in PCK and WT rat serum and urine samples.

Results: The mRNA of Mrp3, Ostα, and Mdr1 was increased by 9-, 120-, and 73-fold, respectively in livers from PCK compared to WT rats. Western blot analysis confirmed Mdr1 upregulation (2.3-fold), and Mrp2 and Oatp1a4 downregulation (3-fold) in PCK rat liver samples. Interestingly, Mrp2 and Mrp4 protein levels in PCK rat kidney increased 3.3- and 2.5-fold, respectively. CP-I and CP-III concentrations were elevated in PCK serum and urine samples, consistent with altered transporter expression in PCK compared to WT rats.

Conclusion: Differences in hepatic and renal transporter expression may contribute to altered drug disposition in PKD and PLD.

Supported by Otsuka Pharmaceutical Development & Commercialization, Inc., and by NIH R01 GM041935, and R35 GM122576.

Functional Screening of Renal Drug Transporters Activity in Cryopreserved Human Proximal Tubule Epithelial Cells

Pedro Pinto, Katherine S. Fenner, Simone H. Stahl
Drug Safety and Metabolism, IMED Biotech Unit, AstraZeneca

Purpose: Renal transport studies *in vitro* are constrained by the loss of native drug transport activity; therefore, cell type choice is crucial for study design. Here we describe a set of assays to determine the functionality of human renal cryopreserved proximal tubule epithelial cells (hPTEC).

Methods: After expansion hPTEC were cultured in 96 well standard (SW) or transwell plates (TW; pore size: 0.4µm). Transporter activity was determined using model fluorescent substrate and inhibitor pairs for Organic Cation Transporter 2 (OCT2; 4-Di-10-ASP/imipramine), Organic Anion Transporters (OATs; fluorescein/probenecid), P-glycoprotein (P-gp; calcein-AM/valspodar), and Multidrug-Resistance Proteins (MRPs; CFDA-SE/MK571). Monolayer integrity (TW) was determined through TEER measurements and Lucifer-Yellow (LY) and FITC-Dextran (70kDa) leakage. Uptake of metformin (±imipramine) and tenofovir (±probenecid) was analyzed using reverse phase LC-MS/MS.

Results: Presence of inhibitors reduced cellular uptake of 4-Di-10-ASP (SP:85±4%; TW:50±18%) and fluorescein (SP:55±17%; TW:45±27%) and increased retention of Calcein-AM (SP:346±26%; TW:366±100%) and CFDA-SE (SP:569±45%; TW:691±77%) compared to control values (100%). In TW format, TEER values were 70±5Ω.cm^2 on day 7 and 139±8Ω.cm^2 on day 10. LY leakage was 6.5±4.3% and absent on day 10, FITC-Dextran did not cross the cell monolayer. Cellular concentrations of tenofovir and metformin were reduced upon inhibition to 53±9% and 45±10%, respectively.

Conclusion: Expanded hPTEC showed considerable activity of key basolateral and apical renal drug transporters, in both SW and TW culture formats, and demonstrated low leakage of marker molecules. This suite of assays can be applied to investigate interactions of drug molecules with transporter function during drug development.

Effects of Single-Nucleotide Variants in the Intracellular Loop 1 (ICL1) of ABCG2

Noora Sjöstedt[1], Ritchie G.M. Timmermans[1], Jeroen J. M. W. van den Heuvel[2], Jan B. Koenderink[2], Heidi Kidron[1]
University of Helsinki, [2]Radboud Institute for Molecular Life Sciences, Radboud University Medical Center

Purpose: The Q141K variant of ABCG2 is known to decrease ABCG2 function and may predispose individuals to gout. Based on the 3D structure of ABCG2, the position of this variant is in close proximity to the coupling helix formed by intracellular loop 1 (ICL1). Interaction between the nucleotide binding domain and ICL1 is important for mediating conformational changes during the transport process. Amino acid changes in these regions may thus impair protein folding or function, as seen with Q141K. Therefore, this study was designed to investigate the effect of single-nucleotide variants in ICL1 on ABCG2 transport function and expression.

Methods: Five naturally occurring, rare single-nucleotide variants in ICL1 of ABCG2 (K453R, I456V, H457R, G462R and G462V) were generated using site-directed mutagenesis. In addition, two common variants (V12M and Q141K) in the nucleotide binding domain were included in the studies as controls. The wild type (WT) and variant proteins were expressed in HEK293 cells using a modified baculovirus expression system. Crude membrane fractions of the cells were extracted to prepare membrane vesicles. The transport activity of the variants was tested using the vesicular transport assay with ABCG2 substrates Lucifer yellow (50 µM) and estrone sulfate (1 µM). The relative expression levels in the membrane vesicles were analyzed using western blotting, and immunofluorescence microscopy was used to study the localization of the variants in the transduced HEK293 cells.

Results: The expression and activity of Q141K and V12M were in line with previous literature reports: Q141K resulted in clear reduction of transport and expression, while V12M caused only a moderate decrease. Of the ICL1 variants, K453R did not cause significant changes in the transport of either substrate. Both variants at position 462 decreased the apparent transport activity of ABCG2 with the G462R showing < 25% and G462V < 5% transport activity compared to WT. Interestingly, I456V increased estrone sulfate transport by 92%, whereas H457R decreased the transport of Lucifer yellow to 33% of WT without affecting the transport of estrone sulfate. The expression of ABCG2 in H457R, G462R and G462V vesicles was considerably lower than in WT vesicles, and based on immunofluorescence microscopy, the localization of these variants to the cell membrane was impaired.

Conclusion: Amino acid changes in the ICL1 of ABCG2 can result in altered expression and activity of ABCG2. The results further highlight the importance of the ICL1 coupling helix for ABCG2 function.

Epigenetic Regulation of the MDR1 Transporter at the Human Blood-Brain Barrier: Interplay Between Histone Acetylation and Aryl Hydrocarbon Receptor Signaling

Dahea You[1], Xia Wen[2,3], Ayeshia Morris[1], Jason R. Richardson[4], Lauren M. Aleksunes[2,3].
[1]Joint Graduate Program in Toxicology, Rutgers University, [2]Environmental and Occupational Health Sciences Institute, Rutgers University, [3]Department of Pharmacology and Toxicology, Rutgers University, [4]Northeast Ohio Medical University

Purpose: To investigate the molecular mechanism by which histone deacetylase (HDAC) inhibitors regulate Multidrug Resistance Protein 1 (MDR1, ABCB1) at the human blood-brain barrier (BBB).

Methods: Immortalized human brain capillary endothelial (hCMEC/D3) cells, a model of the BBB, were treated with six different HDAC inhibitors, valproic acid (VPA), sodium butyrate (NaB), romidepsin, apicidin, suberoylanilide hydroxamic acid (SAHA), and trichostatin A (TSA), and assessed for expression and function of MDR1. Subsequently, the role of the aryl hydrocarbon receptor (AHR) in regulating MDR1 was tested using β-naphthoflavone (BNF), an AHR activator, and CH-223191 (AHRi), an AHR inhibitor, during HDAC inhibition.

Results: HDAC inhibition following treatment was confirmed by increased levels of acetylated histone H3 protein. After 12 h of treatment, VPA, apicidin, SAHA, and TSA up-regulated MDR1 mRNA levels between 50% and 200%. Similarly, the protein expression of MDR1 transporter was up-regulated two-fold at 24 h. Enhanced MDR1 expression corresponded with reduced intracellular accumulation of the substrate rhodamine 123. The up-regulation of MDR1 mRNA by HDAC inhibitors mirrored increases in the mRNA expression of AHR (R2=0.9). At 6 hr, BNF alone had no effect on MDR1 mRNA expression while SAHA increased it by 160%. However, concurrent exposure to both BNF and SAHA induced MDR1 mRNA by 290%. mRNA expression of CYP1A1, a known target of AHR, was also increased to a much greater extent by this combination. At 12 hr, AHRi did not significantly change the basal level of MDR1 mRNA, but attenuated SAHA-mediated induction of MDR1 mRNA by 60%. Induction of CYP1A1 mRNA by SAHA was also significantly reduced by AHRi.

Conclusion: Collectively, these results demonstrate that (1) HDAC inhibition up-regulates MDR1 transporter at the BBB; (2) and AHR is a potential regulator of MDR1 transporter following HDAC inhibition in human blood-brain barrier cells. Epigenetic regulation of MDR1 in BBB cells is a novel mechanism that may restrict the access of xenobiotics to the brain.

Supported by R01ES021800, P30ES005022 and Bristol-Myers Squibb Fellowship.

Effect of a Common Genetic Variant (p.V444A) in the Bile Salt Export Pump on the Kinetics and Inhibition of Bile Acid Transport

Izna Ali[1], Seher Khalid[1], Bruno Stieger[2], Kim L.R. Brouwer[1]
[1] Division of Pharmacotherapy and Experimental Therapeutics, UNC Eshelman School of Pharmacy, University of North Carolina, Chapel Hill, North Carolina, USA.
[2] Department of Clinical Pharmacology and Toxicology, University Hospital Zürich, Zürich, Switzerland.

Purpose: The bile salt export pump (BSEP) is the primary canalicular transporter responsible for the excretion of bile acids from hepatocytes to bile. Taurocholic acid (TCA) is a prototypical bile acid commonly used for *in vitro* studies of BSEP function. A common variant (rs2287622; p.V444A) in the gene encoding for BSEP has been associated with drug-induced cholestasis. However, the kinetic parameters for TCA transport by 444V BSEP (reference) and 444A BSEP (variant) are similar. Individual bile acids may differ in substrate affinity and/or inhibition potency for the variant compared to reference BSEP. Therefore, the purpose of this study was to evaluate the interactions of various bile acids with the variant compared to the reference BSEP.

Methods: Membrane vesicles were generated from baculovirus infected Sf9 cells expressing either variant or reference BSEP. The interaction of various bile acids with the variant and reference protein was studied by measuring their potency as inhibitors of BSEP-mediated TCA transport. Membrane vesicles (10 µg/reaction) were incubated for 2 min with [^{3}H]-TCA (2 µM) in the presence or absence of 4 mM ATP. Deoxycholic acid (DCA), glycochenodeoxycholic acid (GCDCA), glycocholic acid (GCA), lithocholic acid (LCA), and taurochenodeoxycholic acid (TCDCA) were tested as inhibitors of BSEP-mediated TCA transport at a concentration of 100 µM. Based on the results of this initial screen, experiments were conducted to determine the IC_{50} values for the strongest inhibitors. The transport kinetics of GCA also was evaluated by incubating membrane vesicles for 1 min with a range of [^{14}C]-GCA concentrations in the presence or absence of 4 mM ATP to calculate V_{max} and K_m values.

Results: All bile acids tested at 100 µM inhibited both variant and reference BSEP-mediated TCA transport (in descending order from greatest to least inhibition: TCDCA ≈ GCDCA > GCA > DCA ≈ LCA). IC_{50} values (±SE) for the two strongest inhibitors of variant BSEP vs. reference BSEP were 3.60±0.56 vs. 1.83±0.51 µM, respectively, for TCDCA (p=0.14) and 6.27±0.80 vs. 4.33±0.64 µM, respectively, for GCDCA (p=0.32). GCA transport for variant and reference BSEP followed Michaelis-Menten kinetics with V_{max} values of 1217±336 vs. 1298±363 pmol/min/mg protein, respectively, and K_m values of 61.81±32.69 vs. 51.38±31.88 µM, respectively; GCA transport was not significantly different between variant and reference BSEP (p=0.42).

Conclusion: GCDCA and TCDCA were potent inhibitors of TCA transport for both variant and reference BSEP. No significant differences were observed between variant and reference BSEP transport kinetics or inhibition for the bile acids studied.

Supported by NIH R01 GM041935, R35 GM122576, and T32 GM086330

Molecular Interactions and Size Restrictions in the Binding and Transport of Drugs by Human Solute Carriers

Ursula Thormann, Maria Karlgren, Pär Matsson
Department of Pharmacy, Uppsala University

Purpose: To assess differences between the molecular properties of drug molecules that lead to inhibitory binding and those that lead to substrate translocation by human solute carriers (SLCs).

Methods: A database of substrate translocation evidence was collated from online sources and was expanded through manual curation of recent transporter literature. Transport inhibition data were assembled from large, internally consistent literature datasets. In total, the analyses were based on more than 5,000 measurements of ligand binding and substrate translocation. Protein structure data were extracted from the Protein Data Bank (www.rcsb.org) by searching for amino acid sequences homologous to the major human drug-transporting SLCs. Molecular properties of inhibitors and substrates were calculated based on ensembles of low-energy conformations for each molecule, and were compared using univariate descriptor distributions and multivariate structure-property relationships. Human SLC binding sites were modeled through virtual mutation of ligand-interacting residues in the template structures.

Results: Inhibitors were statistically indistinguishable from substrates for all evaluated SLCs with respect to the net molecular charge, suggesting charge-directed interactions with the same or similar binding sites for both types of ligands. In contrast, inhibitors were significantly more lipophilic (mean difference of 2.3±0.4 AlogP units; $p < 1\times10^{-5}$ for all transporters except OATP1B1) and larger (mean difference 82±39 Å^3 in molecular volume; $p < 1\times10^{-4}$) than substrates of the same SLC transporter. Modeling of the binding sites of human SLCs based on crystal structures of homologous transporters indicated binding site volumes in the same range as that observed in reported substrates (<500 Da), but smaller than that seen for many inhibitors.

Conclusion: Collective evidence from structures of SLC ligands and protein structures indicated that binding of inhibitors and substrates might predominantly occur to the same or to chemically similar binding sites. The higher lipophilicity and size among inhibitors suggest hydrophobic interactions and steric restriction to be major drivers in the different binding compared to that of transported substrates.

Interactions of Bile Acids and Liver Injury-associated Drugs with Organic Solute Transporter α/β

James J. Beaudoin[1], Melina M. Malinen[1], Antti S. Kauttonen[1,2], Noora Sjöstedt[1], Paavo Honkakoski[2], Kim L. R. Brouwer[1]

[1]Division of Pharmacotherapy and Experimental Therapeutics, UNC Eshelman School of Pharmacy, University of North Carolina, Chapel Hill, North Carolina, USA; [2]School of Pharmacy, Faculty of Health Sciences, University of Eastern Finland & Biocenter Kuopio, Kuopio, Finland

Purpose: Organic solute transporter (OST) α/β, a heteromeric, basolateral transporter expressed primarily in the liver and intestine, is believed to be vitally important in the homeostasis of bile acids and other steroid hormones. The impact of drug interactions and elevated concentrations of bile acids on the function of OSTα/β is unclear. This knowledge gap may explain, in part, our inability to accurately predict drug-induced liver injury (DILI). The purpose of this study was to identify and quantify the potency of novel inhibitors of OSTα/β-mediated transport from a panel of bile acids and DILI-associated compounds.

Methods: Using Flp-In™ 293 cell lines stably overexpressing human OSTα/β or empty vector, uptake and inhibition studies were performed with [^{3}H]-dehydroepiandrosterone sulfate (DHEAS; 20 μM and 4 μM, respectively) as a steroid substrate. Uptake studies were performed from 5 sec to 30 min to determine the linear range. A total of 73 structurally diverse compounds (100 μM) associated with DILI were screened to identify novel OSTα/β inhibitors. The strongest inhibitors were used in follow-up studies, conducted at five (2-200 μM), six (2-500 μM) or seven (0.125-200 μM) inhibitor concentrations, to determine half-maximal inhibitory concentration (IC_{50}) values.

Results: OSTα/β-mediated DHEAS uptake was linear up to 1 min, in agreement with our previous uptake studies using estrone sulfate and taurocholate. Therefore, inhibition studies were conducted at the 30-sec time point. A total of seven compounds inhibited OSTα/β-mediated DHEAS uptake by >25%, including DILI-associated medications and one bile acid. IC_{50} estimates (μM±SE) were determined for ethinylestradiol (30.7±2.5), fidaxomicin (180.1±23.5), troglitazone sulfate (182.8±22.2), and glycochenodeoxycholate (458.2±137.5). For other compounds, the IC_{50} values could not be determined due to solubility concerns.

Conclusion: Various chemically diverse compounds, including cholestatic DILI drugs and a prevalent bile acid species, are OSTα/β inhibitors *in vitro*. This OSTα/β screening system is useful for rank ordering the potency of inhibitors and calculating IC_{50} values. As with all *in vitro* systems, IC_{50} values are dependent on the assay conditions (*e.g.*, substrate concentration and expression levels of the transporter). Experiments are ongoing to develop computational models to predict novel OSTα/β inhibitors and to elucidate the role of OSTα/β in cholestatic DILI.

Supported by NIH R01 GM041935 and R35 GM122576; the Erasmus+ Programme Global Mobility funds; the Finnish Cultural Foundation and Orion Research Foundation; and the Sigrid Juselius Foundation.

Spatial and Sex Differences in the Intestinal Expression of Monocarboxylate Transporters

Jieyun Cao, Melanie A. Felmlee
Department of Pharmaceutics and Medicinal Chemistry, TJL School of Pharmacy and Health Sciences, University of the Pacific

Purpose: Proton- and sodium-dependent monocarboxylate transporters (MCTs (SLC16A) and SMCTs (SLC5A)) transport monocarboxylates such as ketone bodies, lactate and pyruvate, as well as drugs such as gamma-hydroxybutyric acid. CD147 acts as an ancillary protein for MCT1 and MCT4, and is involved in membrane trafficking. Previous work has demonstrated that hepatic MCT and CD147 expression varies between males and over the estrus cycle in females. The purpose of this study is to evaluate the spatial intestinal mRNA expression of MCT1, MCT4, SMCT1 and CD147 in males, over the estrus cycle in females and in the absence of female sex hormones.

Methods: Intestinal samples (duodenum, jejunum, ileum) were harvested from groups of Sprague-Dawley rats (N = 3 – 5 per group): males, females at the four stages of the estrus cycle (proestrus, estrus, metestrus and diestrus) and ovariectomized (OVX) females. Female estrus cycle stages were classified by vaginal lavage smear. mRNA expression of MCT1, MCT4, SMCT1 and CD147 was quantified by validated qPCR assays and normalized to Alien RNA. Fold-change between groups was determined using the ΔΔCT method.

Results: Significant differences were observed in the spatial expression of MCT1, MCT4, SMCT1 and CD147, and sex differences in MCT1, MCT4 and CD147 as determined by two-way ANOVA. For all four genes, the lowest expression levels were observed in the duodenum: duodenal MCT1, MCT4 and CD147 was ~70-80% lower than in the ileum. The largest spatial differences in expression were observed with SMCT1 with 50 to 75-fold higher expression in the ileum across all groups. Sex differences in expression of MCT1, MCT4 and CD147 were observed in the jejunum and/or ileum, with no sex differences for SMCT1 across all intestinal regions. Expression of MCT1 and CD147 in the jejunum was significantly lower in proestrus, estrus, diestrus and OVX females as compared to males (~70% lower expression). MCT4 expression in the ileum was 3-fold higher in OVX females as compared to females with hormone cycling.

Conclusions: Spatial and region-specific sex differences exist in the intestinal expression of MCTs and SMCTs with the highest expression observed in the ileum. Sex differences in MCT1 and CD147 expression are likely not mediated by sex hormones as OVX expression was consistent with intact females. In contrast, MCT4 expression was increased in OVX females supporting the role of female sex hormones in its regulation. These results differ from the sex-hormone dependent expression of MCT1 and MCT4 observed in the liver suggesting that sex differences in MCT expression are tissue-specific.

The Influence of Dissolution, PMAT Influx, and MATE Efflux Rates on Paracellular Absorption of Metformin Using a Mechanistic Oral Absorption / PBPK Model

Michael B. Bolger, Joyce Macwan, Viera Lukacova
Simulations Plus

Purpose: A physiologically based compartmental absorption and distribution model was developed for metformin to facilitate our understanding of the influence of transporters and dissolution rate on absorption.

Methods: A mechanistic oral absorption / PBPK model for metformin was developed using GastroPlus™ (Simulations Plus, Inc., Lancaster CA). The model incorporated PMAT influx and MATE efflux on the apical membrane of the intestinal lumen, along with paracellular permeability as the only route of absorption into the portal vein. Systemic clearance was modeled by using permeability-limited liver and kidney tissues with the following transporters: OCT1 (basolateral liver influx), OCT2 (basolateral kidney influx), and MATE2K (apical kidney efflux). Transporter Km values were taken directly from *in vitro* literature studies and Vmax values were optimized to fit the observed clinical data. The model was validated by comparing the simulation results to literature data (Tucker 1981, Pentikainen 1979, and Balan 2001) for intravenous and oral administration assuming solution, IR, ER, and XR formulations of metformin administered to human subjects under fed and fasted conditions. The influence of dissolution rate on the rate and extent of metformin absorption was tested by using a variety of intestinal lumen metformin release rates using Weibull function profiles.

Results: A single set of transporter Km and Vmax values implemented in the GastroPlus ACAT model were found to accurately fit all of the human clinical literature data. It was also observed that the rate and extent of absorption was relatively insensitive to the lumenal release rate of metformin. For immediate release formulations, the simulations showed that the relative rates of influx and efflux changed the regional location of paracellular absorption and modified the Tmax, but Cmax and AUC were less sensitive. Simulated absorption for classical extended release formulations resulted in much lower exposure due to the smaller paracellular pore size in the lower GI and colon. However, the simulations for gastric retentive Glucophage XR formulations were bioequivalent with IR formulations.

Conclusions: The mechanistic oral absorption/PBPK model developed for this study is one of the first to include the influence of intestinal apical transporters and paracellular absorption of metformin (see also Kakhi and Lukacova, 2015 AAPS Annual meeting presentation). The model is suitable to help generic formulation development and to test for virtual bioequivalence. The model can also be used for simulations of transporter drug-drug interactions.

Assessing OATP1B1- and OATP1B3-Mediated Drug-Drug Interaction Potential of Vemurafenib Using Static and Physiologically Based Pharmacokinetic Models

T. Farasyn, S. Pahwa, R. Kayesh, K. Alam, K. Ding, W. Yue
University of Oklahoma Health Sciences Center

Purpose: Organic anion transporting polypeptides (OATP) 1B1 and 1B3 are hepatic transport proteins that mediate the uptake of a wide variety of drugs and have been found to be important determinants of transporter-mediated drug-drug interactions (DDIs). Current studies were designed to assess the OATP-mediated DDI potential of vemurafenib, a kinase inhibitor drug with high protein binding and low aqueous solubility, using static R-value and physiologically based pharmacokinetic (PBPK) models.

Methods: Accumulation of [^{3}H]$E_2$17βG (1 μM, 2 min) and [^{3}H]CCK-8 (1 μM, 3 min) was determined in human embryonic kidney (HEK) 293-OATP1B1 and -1B3, respectively. Following the US FDA draft guidance, a 1-h pre-incubation step was included when determining the inhibition of vemurafenib against OATP1B1 and OATP1B3. The total half-maximal inhibitory concentration ($IC_{50,total}$) values of vemurafenib against OATP1B1 and OATP1B3 were determined in HEK293-OATP1B1 and -OATP1B3, respectively, in the presence of 4% (w/v) bovine serum albumin (BSA). The $IC_{50,unbound}$ values were estimated by multiplying the $IC_{50,total}$ values with the reported vemurafenib unbound fraction in buffer ($f_{u,inc}$) of 0.002 or an assumed, conservative $f_{u,inc}$ of 0.01. The inhibitory effects of vemurafenib on OATP1B1 and OATP1B3 were also determined in the absence of BSA. R-Values [$R=1+(f_{u,plasma} \times I_{in,max}/IC_{50})$] were calculated based on the FDA draft guidance for OATP-mediated DDI studies. A vemurafenib PBPK model was developed to assess the OATP-mediated DDI potential using pravastatin as the substrate.

Results: Pre-incubation with vemurafenib at clinically relevant concentrations significantly decreased OATP1B1- and OATP1B3-mediated transport and reduced the $IC_{50,total}$ against both transporters. Vemurafenib $IC_{50,unbound}$ values after pre-incubation were 0.051 and 0.037 μM against OATP1B1 and OATP1B3 estimated with $f_{u,inc}$ of 0.002, yielding area under the concentration-time profile ratio (AUCR)-values of 26.9 and 36.7, respectively, and were 0.25 and 0.19 μM using $f_{u,inc}$ of 0.01, yielding AUCR values of 6.28 and 7.95, respectively. The simulated pravastatin AUC ratio was 2.06 when a single dose of pravastatin (40 mg) was co-administered with vemurafenib (960 mg, twice daily) at steady-state.

Conclusion: Both the static R-value and PBPK models predict that vemurafenib has the potential to cause OATP-mediated DDIs. When determining IC_{50} values, taking protein binding and an inhibitor-pre-incubation into consideration may help to establish the *in vitro-in vivo* correlation for OATP inhibition.

Supported by NIH R01 GM094268